Degenerate helix spin configuration supported by three-site biquadratic exchange

E. Rastelli and A. Tassi
Dipartimento di Fisica, Univerisità di Parma and INFM, 43100 Parma, Italy
(Received 7 February 1995)

Inequivalent Bragg peaks in the same direction were observed in the neutron-scattering cross section of $RbMnBr_3$, a hexagonal antiferromagnet of the ABX_3 family. Here we show that a suitable higher-order exchange interaction, such as a three-site biquadratic exchange, creates significant changes in the phase diagram of a triangular Heisenberg antiferromagnet. Indeed an infinite degeneracy point appears in the neighborhood where two helices coexist characterized by a wave vector in the same direction but with a different turn angle. In addition a *swinging helix* characterized by a wave vector changing continuously in magnitude and direction throughout its stability region is found.

I. INTRODUCTION

A wealth of spin configurations has been found in magnetic insulators in addition to the ferromagnetic and antiferromagnetic ones. Indeed, helix, cone, longitudinally ordered, and multiply periodic structures were experimentally observed and theoretically explained on the basis of suitable exchange interactions and anisotropy terms.[1]

In spite of the many spin configurations already observed, an unexplained magnetic structure was found by elastic neutron scattering on $RbMnBr_3$,[2,3] a hexagonal antiferromagnetic of the ABX_3 family where A is an alkali element, B a magnetic ion, and X a halogen. Indeed, two Bragg peaks at inequivalent wave vectors in the first Brillouin zone were observed at $\mathbf{Q}_{\pm}=(\frac{3}{8}\pm\delta,\frac{3}{8}\pm\delta,\frac{1}{2})$ with $\delta=0.0183$.[2,3] The well-known source of helix spin patterns is the exchange competition and the helix wave vectors $\mathbf{Q}_{\pm}$ might correspond to moderate values of in-plane next-nearest-neighbor (NNN) and third-nearest-neighbor (TNN) competing interactions,[4] but two different sets of exchange parameters must be present in the sample. This hypothesis looks like very artificial so that we propose here a more realistic model that supports two different inequivalent Bragg peaks in the first Brillouin zone.

Here we do not pretend to give a full explanation of the surprising experimental data concerning $RbMnBr_3$. We simply investigate a mechanism able to support coexisting helices characterized by different wave vectors pointing in the same direction. We have identified as a possible source of degenerate helices the three-site biquadratic interaction that couples a spin with two spins of its nearest-neighbor shell. The effect of such an interaction on collinear spin configuration was studied by a random-phase-approximation (RPA) approach.[5] Here we consider the effect of that biquadratic interaction on the helix spin configurations. In particular, we consider a triangular Heisenberg antiferromagnet with a possible lattice distortion that accounts for the elastic Bragg peak observed at $\mathbf{Q}_{+}=(\frac{3}{8}+\delta,\frac{3}{8}+\delta,\frac{1}{2})$.[6] When the biquadratic exchange is introduced we find that incommensurate helices may occur even without lattice distortion. Indeed, the competition between the antiferromagnetic exchange coupling on the triangular lattice that leads to a 120° three-sublattice configuration and the three-site biquadratic exchange that supports collinear configurations is sufficient to yield incommensurate helices.

II. GROUND-STATE CONFIGURATION

Since the strong antiferromagnetic coupling along the c axis in a hexagonal structure assures antiferromagnetic order in this direction we model the system by a triangular lattice for simplicity reasons. Indeed, the configuration of the three-dimensional (3D) model is the same layer by layer as that of the 2D model we consider.

We account for a NN in-plane interaction and a three-site biquadratic exchange interaction. We will show that this higher-order exchange interaction recovers some features of the unusual structure observed in $RbMnBr_3$.

The Hamiltonian we consider reads

$$\mathscr{H}=-\sum_{i\boldsymbol{\delta}} J_{\boldsymbol{\delta}}\mathbf{S}_i\cdot\mathbf{S}_{i+\boldsymbol{\delta}}-\sum_{i\boldsymbol{\delta},\boldsymbol{\delta}'} B_{\boldsymbol{\delta},\boldsymbol{\delta}'}(\mathbf{S}_i\cdot\mathbf{S}_{i+\boldsymbol{\delta}})(\mathbf{S}_i\cdot\mathbf{S}_{i+\boldsymbol{\delta}'}), \tag{2.1}$$

where $\boldsymbol{\delta}$ and $\boldsymbol{\delta}'$ are vectors joining one spin at site i with its six NN's at sites $(\pm a,0,0)$, $(\frac{1}{2}a,\pm(\sqrt{3}/2)a,0)$, and $(-\frac{1}{2}a,\pm(\sqrt{3}/2)a,0)$. $J_{\boldsymbol{\delta}}$ is the exchange coupling and $B_{\boldsymbol{\delta},\boldsymbol{\delta}'}$ is the strength of the three-site interaction involving a spin with two of its NN spins.[5] The influence of this kind of higher-order exchange contribution has been studied only by a RPA approach for collinear configurations, where the main effect was found on the order of the phase transition that is first order for sufficiently large biquadratic interaction.[5]

Here we show that this interaction has dramatic effects on the minimum-energy configuration. We also account for a possible lattice distortion along a line of NN spins[6] in order to account for helical configurations which differ from the 120° three-sublattice configuration one has for $J_{\boldsymbol{\delta}}=J<0$ and $B_{\boldsymbol{\delta},\boldsymbol{\delta}'}=0$. The distortion we consider concerns the two spins at $(\pm a,0,0)$. They are supposed to interact with the central spin via J' whereas the other four spins at $(\pm\frac{1}{2}a,\pm(\sqrt{3}/2)a,0)$ interact with the central spin via J. The biquadratic interaction is assumed to be B when $\boldsymbol{\delta}$ and $\boldsymbol{\delta}'$ are vectors joining the central spin at i with the four spins at $(\pm\frac{1}{2}a,\pm(\sqrt{3}/2)a,0)$; B' when $\boldsymbol{\delta}$ and $\boldsymbol{\delta}'$ join the site i with the spins at $(\pm\frac{1}{2}a,\pm(\sqrt{3}/2)a,0)$ and the spins at $(\pm a,0,0)$,

0163-1829/95/52(17)/12755(5)/$06.00

respectively, and vice versa; B'' when $\boldsymbol{\delta}$ and $\boldsymbol{\delta}'$ are vectors joining the central spin with spins at $(\pm a,0,0)$.

The reduced energy e_0 of the model in classical approximations ($S\to\infty$) reads

$$e_0=\frac{E_0}{2|J|NS^2}=2\cos x\,\cos y+j_A\cos(2x)+b[4\cos^2x\,\cos^2y+4b_1\cos x\,\cos y\,\cos(2x)+b_2\cos^2(2x)], \tag{2.2}$$

where $x=\frac{1}{2}aQ_x$, $y=(\sqrt{3}/2)aQ_y$, $j_A=J'/J$, $b=2BS^2/J$, $b_1=B'/B$, and $b_2=B''/B$. For an undistorted lattice $j_A=1$ and $b_1=b_2=1$.

The minimum-energy conditions are

$$-2\sin x\{\cos y+2j_A\cos x+2b[2\cos x\,\cos^2y+b_1\cos y\,\cos(2x)+4b_1\cos^2x\,\cos y+2b_2\cos x\,\cos(2x)]\}=0, \tag{2.3}$$

$$-2\sin y\,\cos x\{1+2b[2\cos x\,\cos y+b_1\cos(2x)]\}=0. \tag{2.4}$$

The possible solutions are as follows.

(i) The antiferromagnetic configuration (AF) with $x=0$, $y=\pi$ or $x=\pi$, $y=0$ with reduced energy

$$e_{\mathrm{AF}}=-2+j_A+b(4-4b_1+b_2). \tag{2.5}$$

(ii) A helix configuration characterized by a wave vector pointing along a NN row with $y=0$ and x the solution of the equation

$$8bb_2\cos^3x+12bb_1\cos^2x+(2j_A+4b-4bb_2)\cos x+1-2bb_1=0. \tag{2.6}$$

When all roots of Eq. (2.6) are real they correspond to one saddle point and two minima. The minima correspond to two helices we call H_1 and H_1', both characterized by wave vectors pointing along a NN row.

(iii) A helix configuration H_2 is a helix characterized by a wave vector pointing along a NNN row with $x=0$ and y such that

$$\cos y=-\frac{1+2bb_1}{4b} \tag{2.7}$$

with energy

$$e_2=-\frac{1}{4b}+j_A-b_1+b(b_2-b_1^2). \tag{2.8}$$

(iv) A *swinging helix* (SH) configuration where the wave-vector direction changes continuously throughout its stability region according to the equations

$$\cos x=-\sqrt{\frac{1}{2}+\frac{b_1-j_A}{4b(b_2-b_1^2)}}, \tag{2.9}$$

$$\cos y=\frac{1+b_1(b_1-j_A)/(b_2-b_1^2)}{2b\sqrt{2+(b_1-j_A)/b(b_2-b_1^2)}}, \tag{2.10}$$

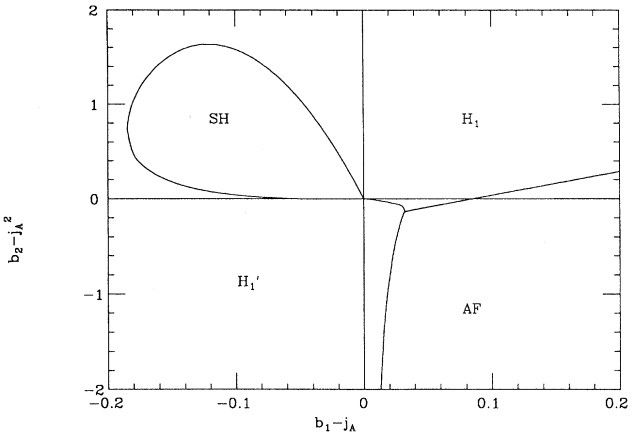

FIG. 1. Phase diagram at $T=0$ for $j_A=1$ and $b=0.35$.

with energy

$$e_{\mathrm{SH}}=-\frac{1}{4b}-\frac{(b_1-j_A)^2}{4b(b_2-b_1^2)}. \tag{2.11}$$

It is reasonable to suppose that $B\simeq J^2$, $B'\simeq JJ'$, and $B''\simeq(J')^2$.

Notice that the SH configuration is present also for the undistorted model ($j_A=1$) provided that $b>\frac{1}{3}$.

Figures 1 and 2 show the zero-temperature phase diagram for $b=0.35$, $j_A=1$ and $b=0.4$, $j_A=1$, respectively. The origin of the phase diagram where $b_1=j_A$, $b_2=j_A^2$ corresponds to an infinitely degenerate ground state as we will show below. As one can see the SH configuration region spreads out very quickly as the three-site biquadratic exchange coupling b increases from 0.35 to 0.4.

The SH-H_1, SH-H_1', and AF-H_1 phase boundaries are second order, whereas the H_1-H_1' and AF-H_1' phase boundaries are first order. On the H_1-H_1' transition line two inequivalent helices coexist. The turn angle characterizing these two coexisting helices runs from 133.5° and 108.1° in the neighborhood of the point H_1-SH-H_1', where infinitely many helices coexist, to 180° and 101.1° at the triple point

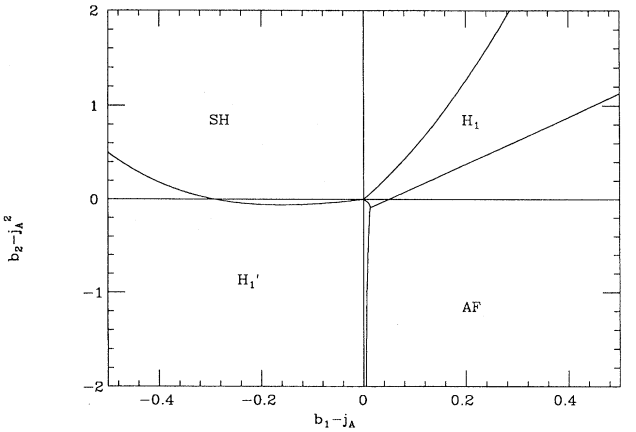

FIG. 2. Phase diagram at $T=0$ for $j_A=1$ and $b=0.4$.

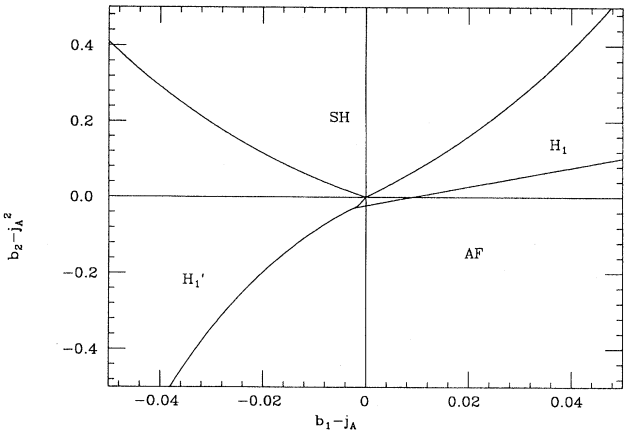

FIG. 3. Phase diagram at $T=0$ for $j_A=2^{-1/2}$ and $b=0.356\,44$.

H_1-AF-H_1' for $b=0.35$ (see Fig. 1). The analogous values for $b=0.4$ are 148.6° and 98.4° at the point H_1-SH-H_1', and 180° and 96.7° at the triple point H_1-AF-H_1'.

Figure 3 shows the phase diagram for $b=0.356\,44$ and $j_A=1/\sqrt{2}$. Notice that for $b=0$ and $j_A=1/\sqrt{2}$ the ground state is a commensurate helix with a turn angle of 135°, the high-field phase observed in $RbMnBr_3$.[2,3] The H_1 and H_1' turn angles for $b=0.356\,44$, $b_1=j_A$, and $b_2=j_A^2$ become 142.9° and 128.1°, respectively. These values correspond to the Bragg peaks observed at $\mathbf{Q}_\pm$ in $RbMnBr_3$. Moving along the H_1-H_1' coexistence line the turn angles of the two phases become 180° and 119.7° at the triple point H_1-AF-H_1'.

Let us focus on the point $b_1=j_A$ and $b_2=j_A^2$ of the phase diagram. At this point conditions (2.3) and (2.4) become

$$-2\sin x(\cos y+2j_A\cos x)\{1+2b[2\cos x\cos y+j_A\cos(2x)]\}=0, \tag{2.12}$$

$$-2\sin y\cos x\{1+2b[2\cos x\cos y+j_A\cos(2x)]\}=0. \tag{2.13}$$

As one can see infinitely many wave vectors minimize the energy. The *infinite-degeneracy* locus in the wave-vector space is

$$1+2b[2\cos x\cos y+j_A\cos(2x)]=0. \tag{2.14}$$

Figures 4 and 5 show the locus of the continuous manifold of wave vectors that minimize the ground-state energy for $j_A=1$ and $j_A=1/\sqrt{2}$, respectively. As one can see in Fig. 4 the infinite-degeneracy locus shrinks to a point for $b=\frac{1}{3}$. For $b<\frac{1}{3}$ the infinite degeneracy disappears. The loci become straight lines for $b=\frac{1}{2}$. The qualitative features are the same for $j_A=1/\sqrt{2}$ as shown in Fig. 5 but the critical value of b is now $b=1/(2\sqrt{2})$. The straight lines occur for $b=1/\sqrt{2}$.

In the vicinity of the infinite-degeneracy point H_1-SH-H_1' the infinite degeneracy disappears but the two helices H_1 and H_1' remain well-defined minima, one being the ground-state configuration, the other being a metastable state.

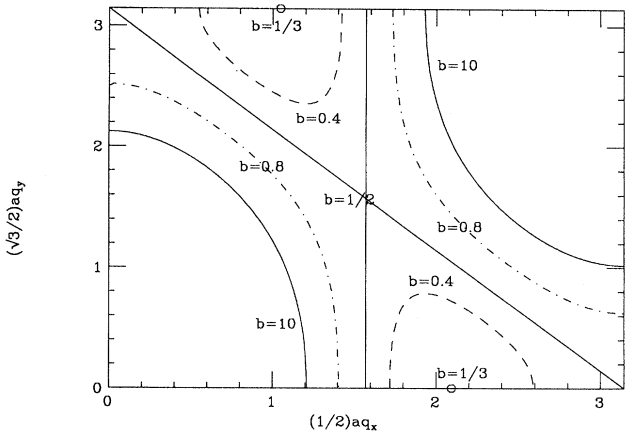

FIG. 4. Infinite-degeneracy wave-vector loci for $j_A=1$ and selected values of b.

III. SPIN WAVES

In order to get the spin-wave spectrum to test the stability of various configurations near the infinite-degeneracy point, we perform the customary steps:[1] introduction of a local quantization axis, spiraling according to a helix of wave vector $\mathbf{Q}$; transformation from spin operators to boson creation and destruction operators keeping only the bilinear contribution; Bogoliubov transformation diagonalizing the bilinear boson Hamiltonian. So doing, Hamiltonian (2.1) becomes

$$\mathcal{H}=E_0+\Delta+\sum_{\mathbf{k}}\hbar\omega_{\mathbf{k}}\alpha_{\mathbf{k}}^\dagger\alpha_{\mathbf{k}}, \tag{3.1}$$

where

$$E_0=-NS^2J(\mathbf{Q})-NS^4B(\mathbf{Q},\mathbf{Q}) \tag{3.2}$$

is the ground-state energy in the classical approximation [see for comparison Eq. (2.2)]. The phase diagram discussed in Sec. II is obtained by minimizing E_0 with respect to $\mathbf{Q}$.

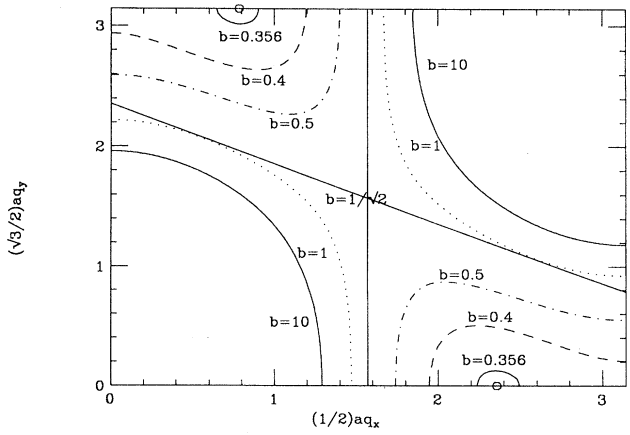

FIG. 5. Infinite-degeneracy wave-vector loci for $j_A=2^{-1/2}$ and selected values of b.

$$\Delta = -NSJ(\mathbf{Q}) - 2NS^3 B(\mathbf{Q},\mathbf{Q}) + \tfrac{1}{2}\sum_{\mathbf{k}} \hbar\omega_{\mathbf{k}} \tag{3.3}$$

is the zero-point-motion energy. $\alpha_{\mathbf{k}}$ is the destruction operator of a magnon of wave vector $\mathbf{k}$ and

$$J(\mathbf{k}) = \sum_{\delta} J_{\delta} \cos(\mathbf{k}\cdot\boldsymbol{\delta}), \tag{3.4}$$

$$B(\mathbf{k},\mathbf{q}) = \sum_{\delta,\delta'} B_{\delta,\delta'} \cos(\mathbf{k}\cdot\boldsymbol{\delta})\cos(\mathbf{q}\cdot\boldsymbol{\delta}'), \tag{3.5}$$

$$\hbar\omega_{\mathbf{k}} = \sqrt{D_{\mathbf{k}} S_{\mathbf{k}}}, \tag{3.6}$$

$$\begin{aligned} D_{\mathbf{k}} = 2S\sum_{\delta} & \cos(\mathbf{Q}\cdot\boldsymbol{\delta})[1-\cos(\mathbf{k}\cdot\boldsymbol{\delta})] \\ & \times\left[J_{\delta} + 2S^2\sum_{\delta'} B_{\delta,\delta'}\cos(\mathbf{Q}\cdot\boldsymbol{\delta}')\right] \\ & - 2S^3\sum_{\delta,\delta'} B_{\delta,\delta'}\sin(\mathbf{Q}\cdot\boldsymbol{\delta}) \\ & \times\sin(\mathbf{Q}\cdot\boldsymbol{\delta}')\sin(\mathbf{k}\cdot\boldsymbol{\delta})\sin(\mathbf{k}\cdot\boldsymbol{\delta}'), \end{aligned} \tag{3.7}$$

$$\begin{aligned} S_{\mathbf{k}} = 2S\sum_{\delta} & [\cos(\mathbf{Q}\cdot\boldsymbol{\delta}) - \cos(\mathbf{k}\cdot\boldsymbol{\delta})] \\ & \times\left[J_{\delta} + 2S^2\sum_{\delta'} B_{\delta,\delta'}\cos(\mathbf{Q}\cdot\boldsymbol{\delta}')\right]. \end{aligned} \tag{3.8}$$

Notice that at the infinite-degeneracy point $b_1 = j_A$, $b_2 = j_A^2$ the magnon spectrum vanishes because Eq. (3.8) becomes the product of two factors one of which coincides with the left side of Eq. (2.14). In this case one has $E_0 = -2|J|NS^2(1/4b)$ and $\Delta = 0$ so that no splitting of the infinite degeneracy occurs even though the first quantum correction is accounted for. The fact that the spectrum vanishes at the infinite-degeneracy point suggests for disorder even though we expect that the long-range order can be recovered by higher-order terms in the expansion of Hamiltonian (2.1) in terms of boson operators.[7]

We are interested in the phases H_1 and H_1' for which the magnon spectrum reads

$$\begin{aligned} D_{\mathbf{k}} = 8|J|S\{ & j_A + 2b[2b_1 X + b_2(2X^2-1)]\} \\ & \times[1-\cos^2 x - 2X^2\cos x(\cos y - \cos x)] \\ & + 2b(1-X^2)[\cos^2 y + 4b_1 X\cos x\cos y + 4b_2 X^2\cos^2 x] \\ & \times(1-\cos^2 x)), \end{aligned} \tag{3.9}$$

$$\begin{aligned} S_{\mathbf{k}} = 8|J|S\{ & j_A + 2b[2b_1 X + b_2(2X^2-1)]\} \\ & \times[X^2 - \cos^2 x - 2X\cos x\cos y], \end{aligned} \tag{3.10}$$

where X is the value of the $\cos x$ solution of Eq. (2.6), $x = \frac{1}{2}ak_x$, and $y = (\sqrt{3}/2)ak_y$.

In Fig. 6 we show the spectra of the configuration H_1 and H_1' along the (1,0) direction for $b = 0.35$, $j_A = 1$, $b_1 = 1.0314$, and $b_2 = 0.9$, a point on the first-order H_1-H_1' phase boundary. Notice the soft modes at the wave vectors corresponding to turn angles of 160.3° and 101.8°, respectively. The soft modes range from 133.5° and 108.1°, in the vicinity of the point $b_1 = j_A = 1$, $b_2 = j_A^2 = 1$, to 180° and 101.5° at the triple point H_1-AF-H_1' (see Fig. 1).

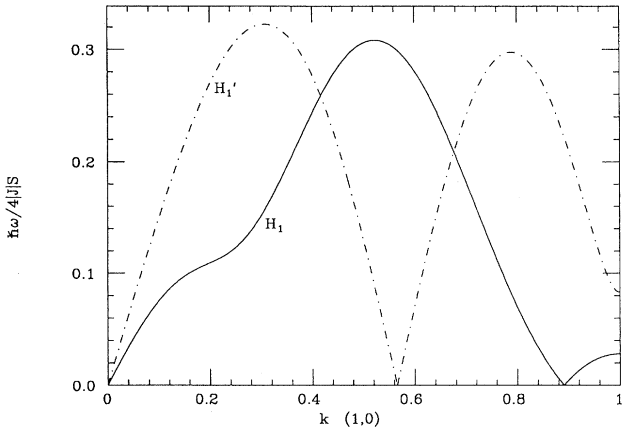

FIG. 6. Spin-wave spectrum along (1,0) direction for $b = 0.35$, $j_A = 1$, $b_1 = 1.0314$, and $b_2 = 0.9$.

In Figs. 7 and 8 we give the spectra of the configuration H_1 and H_1' for $b = 0.4$, $j_A = 1$, $b_1 = 1$, and $b_2 = 0.95$, and for $b = 0.4$, $j_A = 1$, $b_1 = 1.04$, and $b_2 = 1$, respectively. Notice that the former choice of parameters makes the configuration H_1' stable and H_1 metastable, whereas the latter choice makes H_1 stable and H_1' metastable. As one can see the magnon spectrum is well defined also in the metastable phase.

Figure 9 shows the spectra of the configuration H_1 and H_1' for $b = 0.356\,44$, $j_A = 1/\sqrt{2}$, $b_1 = 0.705$, and $b_2 = 0.475$, a point on the H_1-H_1' phase boundary (see Fig. 3). The soft modes range from 142.9° and 128.1°, in the vicinity of $b_1 = j_A = 0.707$, $b_2 = j_A^2 = 0.5$, to 180° and 119.7° at the triple point H_1-AF-H_1'.

In the vicinity of the infinite-degeneracy point the spin-wave spectrum along the (1,0) direction reduces to

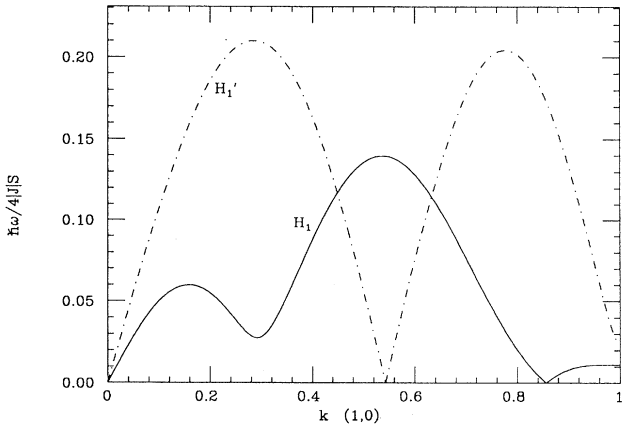

FIG. 7. Spin-wave spectrum along (1,0) direction for $b = 0.4$, $j_A = 1$, $b_1 = 1$, and $b_2 = 0.95$.

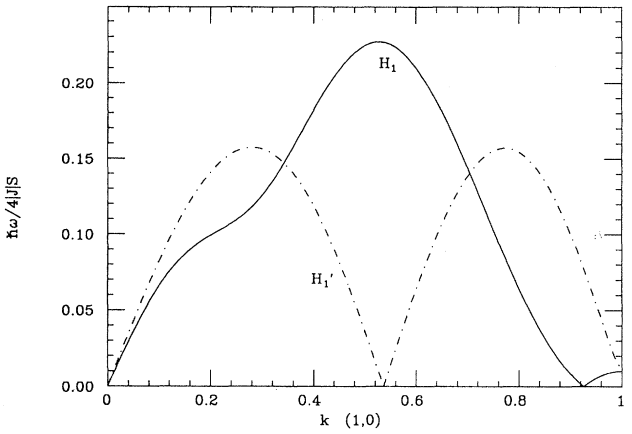

FIG. 8. Spin-wave spectrum along (1,0) direction for $b=0.4$, $j_A=1$, $b_1=1.04$, and $b_2=1$.

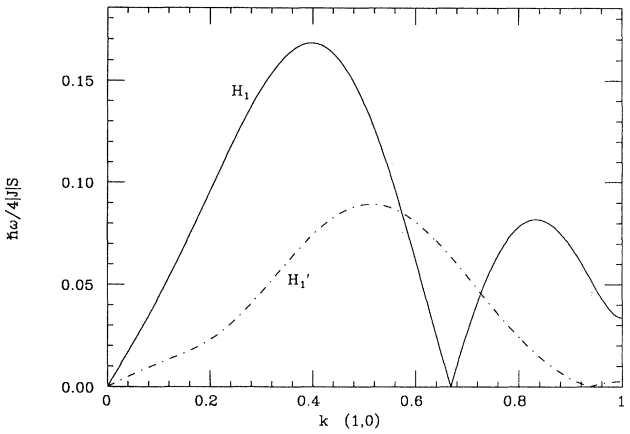

FIG. 9. Spin-wave spectrum along (1,0) direction for $b=0.356\,44$, $j_A=2^{-1/2}$, $b_1=0.705$, and $b_2=0.475$.

$$\hbar\omega_{\mathbf{k}} \simeq 16|J|Sb|\sin x(X-\cos x)(1+2j_A X\cos x)|\sqrt{1-X^2} \times\left[\frac{-j_A(2X^2-1)+2X}{1+2j_A X}(b_1-j_A) + \frac{2X^2-1}{1+2j_A X}(b_2-j_A^2)\right]^{1/2} \tag{3.11}$$

where

$$X=-\frac{1}{2j_A}-\frac{1}{2}\sqrt{2+\frac{1}{j_A^2}-\frac{1}{bj_A}} \tag{3.12}$$

for the phase H_1 and

$$X=-\frac{1}{2j_A}+\frac{1}{2}\sqrt{2+\frac{1}{j_A^2}-\frac{1}{bj_A}} \tag{3.13}$$

for the phase H_1'.

Notice the existence of the soft modes (Goldstone modes) at $x=0$ and $\cos^{-1}X$ and "quasisoft" modes at $x=\pi$ and (for the H_1 phase) at $x=\cos^{-1}(-1/2j_A X)$. The Goldstone modes are a well-known consequence of the symmetry of the Hamiltonian. The "quasisoft" modes disappear if we account for second-order terms in b_1-j_A and $b_2-j_A^2$ in Eq. (3.11). In particular, for $j_A=1/\sqrt{2}$ and $b=0.356\,44$ the Goldstone modes occur at $x=0$ and $0.793\,63\pi$ (corresponding to a turn angle of 142.8°) for the phase H_1 and $x=0$ and $0.711\,70\pi$ (corresponding to a turn angle of 128.1°) for the phase H_1'. The "quasisoft" modes occur at $x=0.152\,72\pi$ (corresponding to a turn angle of 27.5°) for the phase H_1 and $x=\pi$ (zone boundary) for both phases.

IV. SUMMARY

The influence of a three-site biquadratic exchange on the ground-state configuration and on the spin-wave spectrum of a triangular Heisenberg antiferromagnet is considered in Secs. II and III, respectively.

This higher-order exchange interaction was previously studied in the presence of a collinear spin configuration, whereas we consider generic helix configurations. We find the coexistence of different helices H_1 and H_1' (see Figs. 1–3) with different magnitude but the same direction of the helix wave vectors. This could be of interest to explain the unusual elastic-neutron-scattering data of $RbMnBr_3$ where inequivalent Bragg peaks in the same direction were observed. Also, we have found a *swinging helix* characterized by a helix wave vector that changes continuously in magnitude and direction throughout its stability region.

Moreover, the point H_1-SH-H_1' is an infinite-degeneracy point where infinite inequivalent helices minimize the energy of the model. In Sec. III we study the spin-wave spectrum with particular interest in the neighborhood of the H_1-H_1' first-order phase boundary. We find that the spin-wave spectrum is well defined, so providing that H_1' can exist as a metastable configuration where H_1 is stable and vice versa.

[1] J. Jensen and A. R. Mackintosh, *Rare Earth Magnetism. Structures and Excitations* (Clarendon, Oxford, 1991).
[2] L. Heller, M. F. Collins, Y. S. Yang, and B. Collier, Phys. Rev. B **49**, 1104 (1994).
[3] T. Kato, T. Ishii, Y. Ajiro, T. Asano, and S. Kawano, J. Phys. Soc. Jpn. **62**, 3384 (1993).
[4] E. Rastelli and A. Tassi, Z. Phys. B **97**, 147 (1995)
[5] J. Adler and J. Oitmaa, J. Phys. C **12**, 575 (1979).
[6] T. Kato, K. Ito, T. Hoshino, T. Mitsui, and H. Tanaka, J. Phys. Soc. Jpn. **61**, 275 (1992).
[7] E. Rastelli, S. Sedazzari, and A. Tassi, J. Phys. Condens. Matter **3**, 5861 (1991).